Geophys. J. Int. (2004) **159,** 667–678 doi: 10.1111/j.1365-246X.2004.02415.x

Decomposition of the elastic tensor and geophysical applications

Jules Thomas Browaeys[1] and Sébastien Chevrot[2]

[1]*Laboratoire de Dynamique des Systèmes Géologiques, CNRS, UMR* 7579, *Institut de Physique du Globe, Paris, France. E-mail: browaeys@ipgp.jussieu.fr*
[2]*Laboratoire de Dynamique Terrestre et Planétaire, CNRS, UMR* 5562, *Observatoire Midi-Pyrénées, Toulouse, France. E-mail: Sebastien.Chevrot@cnes.fr*

Accepted 2004 June 14. Received 2004 June 14; in original form 2003 November 10

SUMMARY

Elasticity is described in general by a fourth-order tensor with 21 independent coefficients, which corresponds to the triclinic symmetry class. However seismological observations are usually explained with a higher order of symmetry using fewer parameters. We propose an analytical method to decompose the elastic tensor into a sum of orthogonal tensors belonging to the different symmetry classes. The method relies on a vectorial description of the elastic tensor. Any symmetry class constitutes a subspace of a class of lower symmetry and an orthogonal projection on this subspace removes the lower symmetry part. Orthogonal projectors on each higher symmetry class are given explicitly. In addition, the method provides optimal higher symmetry approximations, which allow us to decrease the number of independent parameters. Consequences of the symmetry approximation of the elastic tensor on shear wave splitting (SWS) are investigated for upper-mantle minerals (olivine and enstatite), natural samples and numerically deformed olivine aggregates. The orthorhombic part of the elastic tensor as well as the presence of enstatite are important second-order effects.

Key words: elastic tensor, seismic anisotropy, symmetry class, upper mantle.

1 INTRODUCTION

Seismic anisotropy in the upper mantle of the Earth results mainly from lattice preferred orientation (LPO) of its main constitutive minerals, olivine and orthopyroxene, which are strongly anisotropic (Nicolas & Christensen 1987). Because LPO is produced by deformation of rocks, observations of seismic anisotropy can be used to constrain the pattern of convective flow in the mantle (Ribe 1992; Zhang & Karato 1995).

Different seismic waves are used to study mantle anisotropy. Inversions of surface wave data yield 3-D images of anisotropy with typical lateral and vertical resolutions of 1000 and 100 km, respectively (Montagner & Nataf 1986, 1988; Montagner & Tanimoto 1991; Trampert & Woodhouse 1995). In contrast, shear wave splitting (SWS) measurements provide precise estimates of the polarization direction of the fast *S* wave and *S* delay time beneath receivers, but have poor depth resolution (Silver & Chan 1991; Favier & Chevrot 2003). These different approaches share a need for restrictive simplifying assumptions about the symmetry of the anisotropic medium to ensure tractability. In the case of surface waves, an artificial distinction is made between azimuthal anisotropy (Smith & Dahlen 1973) that uses a horizontal hexagonal axis and radial anisotropy that assumes hexagonal symmetry with a vertical axis (an elastic medium with hexagonal symmetry is equivalent to a transversely isotropic medium). Studies of SWS generally use a small number of uniform hexagonal layers with a horizontal symmetry axis. While such assumptions may be reasonable far from plate boundaries, they are probably invalid in regions such as ridges, hotspots and subduction zones where mantle flow is likely to generate complex variations of anisotropy over short length scales (Kaminski & Ribe 2002).

A promising approach is forward modelling of anisotropy produced by mantle flow using polycrystalline plasticity models (Wenk & Tomé 1999; Kaminski & Ribe 2001). Such calculations yield the anisotropic elastic tensor at all points in the domain under study, from which synthetic seismograms may be calculated and compared with observations (Blackman *et al.* 2002a; Blackman & Kendall 2002b). This approach requires no ad hoc assumptions about the relation between LPO and flow and, in principle, the comparison between predictions and observations should help discriminate between candidate geodynamic models. The determination of the symmetry of the predicted elastic tensor can help in evaluating whether simplified elastic models assumed in inverse problems (e.g., a hexagonal medium with a horizontal symmetry axis) are appropriate representations of the more complicated geodynamic structures. An analysis of the symmetry of elastic tensors calculated from LPO observed in natural samples (Mainprice & Silver 1993) allows also to compare the latter more effectively with numerically predicted elastic tensors. Because seismologists are used to describing seismic anisotropy in terms of orientation of the symmetry axis and amplitude of anisotropy, it is useful to make use of a method to find a representation of any elastic tensor in terms of an optimal hexagonal elastic medium. More generally, we will show that any elastic tensor can be decomposed into contributions corresponding to different symmetry classes.

We introduce an analytical method for the symmetry decomposition of elastic tensors based upon orthogonal projections on subspaces. The representation of the fourth-order elastic tensor by a second-order tensor, preserving its mathematical properties, was first proposed by Kelvin (1856). Unfortunately, this convenient mathematical description is less popular than the widespread Voigt representation (Helbig 1994). Symmetry of the elastic tensor becomes visible when it is expressed in its natural coordinate system whose axes correspond to directions of symmetry. In a pioneering study, Cowin & Mehrabadi (1987) proposed a method for finding the normals to the symmetry planes of the elastic tensor. Arts *et al.* (1991) introduced an analytical method to find the optimal approximation of a given symmetry class for any elastic tensor. They use the coordinate system obtained by the method of Cowin & Mehrabadi (1987) and minimize the distance between the tensor and its representation in a given symmetry class. This gives a system of linear equations for the approximate elastic coefficients. This method is effective for media close to orthorhombic or of higher symmetry. Helbig (1995) proposed the representation of fourth-order elastic tensors by vectors in a 21-dimensional vector space. Using this representation, approximations of the elastic tensor can be seen as projections onto a subspace describing a higher symmetry tensor.

In this article, we extend the approach of Arts *et al.* (1991); Arts (1993) and Helbig (1995) in order to present a practical method that realizes these approximations. We first describe the vectorial representation of elastic tensors and the projections that allow to pass from a given symmetry to any higher order symmetry class. An exact and practical version of the elastic tensor approximation method is formulated. Finally, we consider various applications of the decomposition method to geophysical problems and investigate the consequences of symmetry approximations using materials representative of the upper mantle.

2 FROM THE ELASTIC TENSOR TO THE ELASTIC VECTOR

Elastic properties are mathematically described by Hooke's law, which relates deformation to stress through a fourth-order elastic tensor described by 81 coefficients. The symmetry of the stress tensor σ_{ij} and the strain tensor ε_{ij} reduces the number of independent elastic coefficients from 81 to 36 and the requirement that the elastic energy be completely defined by the strain tensor or the stress tensor further decreases this number to 21 for a triclinic medium. Media with higher symmetry require fewer parameters for their description. A convenient representation of the elastic coefficients is the so-called Voigt notation. The Voigt matrix is a six-dimensional symmetric array C_{IJ} whose elements are related to the c_{ijkl} according to the rules:

$$C_{IJ} = c_{ijkl} \quad \text{with} \quad \begin{cases} I = i\delta_{ij} + (1-\delta_{ij})(9-i-j) \\ J = k\delta_{kl} + (1-\delta_{kl})(9-k-l). \end{cases} \tag{2.1}$$

The Voigt matrix is however not a tensor and no longer preserves the mathematical properties of c_{ijkl}. For elasticity, there are eight distinct symmetry classes: triclinic, monoclinic, orthorhombic, tetragonal, trigonal, hexagonal, cubic and isotropic. A higher symmetry class can be seen as a special case of a lower symmetry class, defined by additional relationships between coefficients (Helbig 1995). Increasing the symmetry of a medium by adding symmetry planes decreases the number of independent parameters.

A useful representation of elastic tensors is in terms of vectors in a 21-dimensional vectorial space. The basis vectors correspond to 21 elementary tensors $\boldsymbol{c}^{(1)}, \ldots, \boldsymbol{c}^{(21)}$ as shown in Table 1. Any elastic tensor can be represented as an elastic vector $\mathbf{X}$ whose components are:

$$\begin{aligned} {}^t\mathbf{X} &= \left(C_{11}, C_{22}, C_{33}, \sqrt{2}C_{23}, \sqrt{2}C_{13}, \sqrt{2}C_{12}, 2C_{44}, 2C_{55}, 2C_{66}, 2C_{14}, 2C_{25}, 2C_{36}, 2C_{34}, 2C_{15}, 2C_{26}, 2C_{24}, 2C_{35}, 2C_{16}, 2\sqrt{2}C_{56}, 2\sqrt{2}C_{46}, 2\sqrt{2}C_{45}\right) \\ &= (X_1, X_2, X_3, X_4, X_5, X_6, X_7, X_8, X_9, X_{10}, X_{11}, X_{12}, X_{13}, X_{14}, X_{15}, X_{16}, X_{17}, X_{18}, X_{19}, X_{20}, X_{21}). \end{aligned} \tag{2.2}$$

The normalization factors that appear in the above expression reflect the multiplicity of the elastic tensor components and are included so that the Euclidean norm of an arbitrary elastic tensor $\boldsymbol{c}$ and its associated elastic vector $\mathbf{X}$ are identical. These norms are defined by

$$N(\boldsymbol{c}) = \sqrt{\langle \boldsymbol{c}, \boldsymbol{c} \rangle} = \sqrt{\langle \mathbf{X}, \mathbf{X} \rangle} = N(\mathbf{X}), \tag{2.3}$$

where the scalar product of arbitrary tensors $\boldsymbol{c}^{(1)}$ and $\boldsymbol{c}^{(2)}$ or their associated vectors $\mathbf{X}^{(1)}$ and $\mathbf{X}^{(2)}$ is

$$\left\langle \boldsymbol{c}^{(1)}, \boldsymbol{c}^{(2)} \right\rangle = c^{(1)}_{ijkl} c^{(2)}_{ijkl} = X^{(1)}_i X^{(2)}_i = \left\langle \mathbf{X}^{(1)}, \mathbf{X}^{(2)} \right\rangle. \tag{2.4}$$

3 DECOMPOSITION OF THE ELASTIC TENSOR BY PROJECTION

3.1 Principle of the orthogonal projection method

A projector in the 21-D elastic vectorial space is described by a 21×21 matrix. Let us consider the elastic vector $\mathbf{X}$ that belongs to a subspace S of dimension N_S of the 21-D vectorial space. A higher symmetry class corresponds to a subspace H of S. Therefore, the elastic vector $\mathbf{X}$ can be decomposed as

$$\mathbf{X} = \mathbf{X}_H + \mathbf{X}_D, \tag{3.1}$$

Table 1. Definition of the elementary tensors $\boldsymbol{c}^{(1)}, \ldots, \boldsymbol{c}^{(21)}$ associated to the 21 orthonormal basis vectors. Voigt matrix elements are also shown.

Fourth-order tensor	Non-zero c_{ijkl} elements	Non-zero C_{IJ} elements
$\boldsymbol{c}^{(1)}$	$c_{1111} = 1$	$C_{11} = 1$
$\boldsymbol{c}^{(2)}$	$c_{2222} = 1$	$C_{22} = 1$
$\boldsymbol{c}^{(3)}$	$c_{3333} = 1$	$C_{33} = 1$
$\boldsymbol{c}^{(4)}$	$c_{2233} = c_{3322} = 1/\sqrt{2}$	$C_{23} = C_{32} = 1/\sqrt{2}$
$\boldsymbol{c}^{(5)}$	$c_{1133} = c_{3311} = 1/\sqrt{2}$	$C_{13} = C_{31} = 1/\sqrt{2}$
$\boldsymbol{c}^{(6)}$	$c_{1122} = c_{2211} = 1/\sqrt{2}$	$C_{12} = C_{21} = 1/\sqrt{2}$
$\boldsymbol{c}^{(7)}$	$c_{2323} = c_{2332} = c_{3223} = c_{3232} = 1/2$	$C_{44} = 1/2$
$\boldsymbol{c}^{(8)}$	$c_{1313} = c_{1331} = c_{3113} = c_{3131} = 1/2$	$C_{55} = 1/2$
$\boldsymbol{c}^{(9)}$	$c_{1212} = c_{2332} = c_{2112} = c_{2121} = 1/2$	$C_{66} = 1/2$
$\boldsymbol{c}^{(10)}$	$c_{1123} = c_{1132} = c_{2311} = c_{3211} = 1/2$	$C_{14} = C_{41} = 1/2$
$\boldsymbol{c}^{(11)}$	$c_{2213} = c_{2231} = c_{1322} = c_{3122} = 1/2$	$C_{25} = C_{52} = 1/2$
$\boldsymbol{c}^{(12)}$	$c_{3312} = c_{3321} = c_{1233} = c_{2133} = 1/2$	$C_{36} = C_{63} = 1/2$
$\boldsymbol{c}^{(13)}$	$c_{3323} = c_{3332} = c_{2333} = c_{3233} = 1/2$	$C_{34} = C_{43} = 1/2$
$\boldsymbol{c}^{(14)}$	$c_{1113} = c_{1131} = c_{1311} = c_{3111} = 1/2$	$C_{15} = C_{51} = 1/2$
$\boldsymbol{c}^{(15)}$	$c_{2212} = c_{2221} = c_{1222} = c_{2122} = 1/2$	$C_{26} = C_{62} = 1/2$
$\boldsymbol{c}^{(16)}$	$c_{2223} = c_{2232} = c_{2322} = c_{3222} = 1/2$	$C_{24} = C_{42} = 1/2$
$\boldsymbol{c}^{(17)}$	$c_{3313} = c_{3331} = c_{1333} = c_{3133} = 1/2$	$C_{35} = C_{53} = 1/2$
$\boldsymbol{c}^{(18)}$	$c_{1112} = c_{1121} = c_{1211} = c_{2111} = 1/2$	$C_{16} = C_{61} = 1/2$
$\boldsymbol{c}^{(19)}$	$c_{1312} = c_{1321} = c_{3112} = c_{3121} = c_{1213} = c_{1231} = c_{2113} = c_{2131} = (2\sqrt{2})^{-1}$	$C_{56} = C_{65} = (2\sqrt{2})^{-1}$
$\boldsymbol{c}^{(20)}$	$c_{2312} = c_{2321} = c_{3212} = c_{3221} = c_{1223} = c_{1232} = c_{2123} = c_{2132} = (2\sqrt{2})^{-1}$	$C_{46} = C_{64} = (2\sqrt{2})^{-1}$
$\boldsymbol{c}^{(21)}$	$c_{2313} = c_{2331} = c_{3213} = c_{3231} = c_{1323} = c_{1332} = c_{3123} = c_{3132} = (2\sqrt{2})^{-1}$	$C_{45} = C_{54} = (2\sqrt{2})^{-1}$

where $\mathbf{X}_H$ belongs to H and the deviation vector $\mathbf{X}_D$ to the subspace orthogonal to H (Helbig 1995). Let p denote an orthogonal projector from subspace S onto subspace H. If $(\mathbf{S}_1, \ldots, \mathbf{S}_{N_S})$ is an orthonormal basis of the subspace S with $(\mathbf{S}_1, \ldots, \mathbf{S}_{N_H})$ belonging to H and $(\mathbf{S}_{N_H+1}, \ldots, \mathbf{S}_{N_S})$ to the subspace orthogonal to H, the deviation vector $\mathbf{X}_D$ constituting the lower symmetry part of the vector is given by

$$\mathbf{X}_D = (\mathbf{X} \cdot \mathbf{S}_{N_H+1})\mathbf{S}_{N_H+1} + \cdots + (\mathbf{X} \cdot \mathbf{S}_{N_S})\mathbf{S}_{N_S} \tag{3.2}$$

and the projector on subspace H is defined by

$$p(\mathbf{X}) = I(\mathbf{X}) - (\mathbf{X} \cdot \mathbf{X}_D)\mathbf{X}_D = \mathbf{X}_H, \tag{3.3}$$

where I is the identity operator. The specific relationships satisfied by the coefficients of a vector that lies in the subspace H allow one to find the set of vectors $(\mathbf{S}_{N_H+1}, \ldots, \mathbf{S}_{N_S})$ that are orthogonal to H. This set is completed by $(\mathbf{S}_1, \ldots, \mathbf{S}_{N_H})$ belonging to H in order to give an appropriate orthonormal basis of S for the projection on H.

We explain in Appendix A how to calculate elementary projectors corresponding to a projection from a symmetry class to the next higher order symmetry class. We then give matrix expressions of more general projectors from any symmetry class onto a higher symmetry class by composing elementary projectors.

3.2 Symmetry cartesian coordinate system

The norm and scalar product defined by eqs (2.3) and (2.4) are invariant under rotation of the 3-D cartesian coordinate system. However, the coefficients of the 21-D vector $\mathbf{X}$ depend both on the 3-D cartesian coordinate system and on the decomposition method. Finding the appropriate 3-D cartesian coordinate system for the projection method requires one to determine the orientations of the symmetry elements.

Cowin & Mehrabadi (1987) define necessary and sufficient conditions for a vector to be normal to a symmetry plane. In particular, they demonstrate that such a vector must be an eigenvector of both the dilatational stiffness tensor $d_{ij} = c_{ijkk}$ and the Voigt stiffness tensor $v_{ik} = c_{ijkj}$, which are given by

$$\mathbf{d} = \begin{bmatrix} C_{11}+C_{12}+C_{13} & C_{16}+C_{26}+C_{36} & C_{15}+C_{25}+C_{35} \\ C_{16}+C_{26}+C_{36} & C_{12}+C_{22}+C_{32} & C_{14}+C_{24}+C_{34} \\ C_{15}+C_{25}+C_{35} & C_{14}+C_{24}+C_{34} & C_{13}+C_{23}+c_{33} \end{bmatrix}, \tag{3.4}$$

Table 2. Structure of the eigenspaces of d_{ij} and v_{ik} and the relation with the symmetry cartesian coordinate system (SCCS) for the different symmetry classes.

Elastic symmetry class	Distinct eigenvalues of d_{ij} & v_{ik}	Coincident eigenvectors of d_{ij} & v_{ik}	Symmetry cartesian coordinate axes
Triclinic	3	0	No particularity
Monoclinic	3	1	Three-axis is the single common eigenvector
Orthorhombic	3	3	Axes are the three common eigenvectors
Tetragonal	2	3	Three-axis is the non-degenerate eigenvector
Hexagonal	2	3	Three-axis is the non-degenerate eigenvector
Isotropic	1	3	No particularity

$$\mathbf{v} = \begin{bmatrix} C_{11}+C_{66}+C_{55} & C_{16}+C_{26}+C_{45} & C_{15}+C_{35}+C_{46} \\ C_{16}+C_{26}+C_{45} & C_{66}+C_{22}+C_{44} & C_{24}+C_{34}+C_{56} \\ C_{15}+C_{35}+C_{46} & C_{24}+C_{34}+C_{56} & C_{55}+C_{44}+C_{33} \end{bmatrix}. \tag{3.5}$$

While a general fourth-order tensor has six distinct contractions of rank two, the symmetries of elastic tensors reduce the number of distinct contractions to two, which are conventionally chosen to be d_{ij} and v_{ik} (Helbig 1994). Physically, the principal directions of d_{ij} are the principal directions of the stress tensor $\sigma_{ij}^{(d)}$ required to produce an isotropic dilatation $\varepsilon_{ij} = \epsilon\delta_{ij}$ of the anisotropic medium:

$$\sigma_{ij}^{(d)} = c_{ijkl}\varepsilon_{kl} = c_{ijkl}\epsilon\delta_{kl} = \epsilon d_{ij}. \tag{3.6}$$

The three principal directions of v_{ik} are the three phase propagation directions corresponding to extreme of the quantity

$$Q = \rho\left(V_P^2 + V_{S1}^2 + V_{S2}^2\right), \tag{3.7}$$

where ρ is the density and V_P, V_{S1} and V_{S2} are the phase velocities of P wave, fast S wave and slow S wave, respectively. Table 2 describes the structure of the eigenspaces of d_{ij} and v_{ik} and the relation between the symmetry cartesian coordinate system (SCCS) and the eigenvectors for the different symmetry classes. For media with orthorhombic or higher symmetry, the eigenvectors of d_{ij} and v_{ik} are identical and define uniquely the SCCS (Bennett 1972; Helbig 1994). For an orthorhombic medium, the three eigenvectors are normal to the three perpendicular symmetry planes. For tetragonal and hexagonal media, only two of the eigenvalues are distinct. Accordingly, the only well-defined axis is the one along the non-degenerate eigenvector, which corresponds to the $2\pi/4$ symmetry axis (tetragonal) or the transverse isotropy axis (hexagonal). The choice of the other two axes is arbitrary. All three axes are arbitrary for an isotropic medium, for which any vector is an eigenvector of both d_{ij} and v_{ik}. A monoclinic medium has a single eigenvector common to d_{ij} and v_{ik}, which is normal to the unique symmetry plane. Finally, a triclinic medium has no eigenvalues common to d_{ij} and v_{ik}, and the choice of the SCCS is arbitrary. For a symmetry lower than orthorhombic, the three SCCS directions are chosen as the bisectrix of each pair of one d_{ij} eigenvector and the corresponding closest v_{ik} eigenvector. This choice is appropriate and stable for a small triclinic part (less than 2–3 per cent) (Arts 1993).

3.3 Decomposition of the elastic tensor

Any triclinic vector $\mathbf{X}$ in a given 3-D cartesian coordinate system can be decomposed by a cascade of projections into a sum of vectors belonging to the different symmetry classes:

$$\mathbf{X} = \mathbf{X}_{\text{tric}} + \mathbf{X}_{\text{mon}} + \mathbf{X}_{\text{ort}} + \mathbf{X}_{\text{tet}} + \mathbf{X}_{\text{hex}} + \mathbf{X}_{\text{iso}}. \tag{3.8}$$

The space of elastic vectors has a finite dimension and thus all correctly defined norms are mathematically equivalent, i.e. using a different norm from eq. (2.3) will change distances but not the resulting decomposition. Moreover, as noted above, an important property of an orthogonal projection is that the distance between a vector $\mathbf{X}$ and its orthogonal projection $\mathbf{X}_H = p(\mathbf{X})$ on a given subspace is minimum. These two features ensure that the decomposition is optimal once the 3-D Cartesian coordinate system is chosen.

4 GEOPHYSICAL APPLICATIONS

In this section, we present the symmetry decomposition of elastic tensors for three classes of media representative (supposedly) of the upper mantle: single crystals of olivine and enstatite, natural peridotite samples from the Kaapvaal craton in Africa, and olivine and enstatite aggregates deformed numerically in a polycrystalline plasticity code. We also investigate the relation between SWS, finite strain and the hexagonal symmetry assumption. The SCCS directions indexes are chosen such that the 3-axis is always the hexagonal axis.

4.1 Decomposition of olivine and enstatite elastic tensors

According to mineralogical models of the upper mantle, olivine is the most abundant (∼70 per cent) and most deformable mineral, while orthopyroxene is the secondary major mineral (∼30 per cent; Anderson 1989). Elastic coefficients are taken from Anderson & Isaak (1995) for olivine $Fo_{90}Fa_{10}$ at 1500 K and from Bass (1995) for enstatite $MgSiO_3$ at room pressure and temperature.

4.1.1 Olivine

The decomposition of the olivine elastic tensor in the different symmetry components is presented below in Voigt notation with elastic coefficients in GPa:

$$C_{IJ} = \begin{pmatrix} 192 & 66 & 60 & 0 & 0 & 0 \\ 66 & 160 & 56 & 0 & 0 & 0 \\ 60 & 56 & 272 & 0 & 0 & 0 \\ 0 & 0 & 0 & 60 & 0 & 0 \\ 0 & 0 & 0 & 0 & 62 & 0 \\ 0 & 0 & 0 & 0 & 0 & 49 \end{pmatrix} = \begin{pmatrix} 16 & 0 & 2 & 0 & 0 & 0 \\ 0 & -16 & -2 & 0 & 0 & 0 \\ 2 & -2 & 0 & 0 & 0 & 0 \\ 0 & 0 & 0 & -1 & 0 & 0 \\ 0 & 0 & 0 & 0 & 1 & 0 \\ 0 & 0 & 0 & 0 & 0 & 0 \end{pmatrix}_{\mathrm{O}}$$

$$+ \begin{pmatrix} 3 & -3 & 0 & 0 & 0 & 0 \\ -3 & 3 & 0 & 0 & 0 & 0 \\ 0 & 0 & 0 & 0 & 0 & 0 \\ 0 & 0 & 0 & 0 & 0 & 0 \\ 0 & 0 & 0 & 0 & 0 & 0 \\ 0 & 0 & 0 & 0 & 0 & -3 \end{pmatrix}_{\mathrm{T}} + \begin{pmatrix} -21.7 & 1.7 & -9.3 & 0 & 0 & 0 \\ 1.7 & -21.7 & -9.3 & 0 & 0 & 0 \\ -9.3 & -9.3 & 77.3 & 0 & 0 & 0 \\ 0 & 0 & 0 & -2.7 & 0 & 0 \\ 0 & 0 & 0 & 0 & -2.7 & 0 \\ 0 & 0 & 0 & 0 & 0 & -11.7 \end{pmatrix}_{\mathrm{H}} + \begin{pmatrix} 194.7 & 67.3 & 67.3 & 0 & 0 & 0 \\ 67.3 & 194.7 & 67.3 & 0 & 0 & 0 \\ 67.3 & 67.3 & 194.7 & 0 & 0 & 0 \\ 0 & 0 & 0 & 63.7 & 0 & 0 \\ 0 & 0 & 0 & 0 & 63.7 & 0 \\ 0 & 0 & 0 & 0 & 0 & 63.7 \end{pmatrix}_{\mathrm{I}}.$$

Subscripts are O for orthorhombic, T for tetragonal, H for hexagonal and I for isotropic. The isotropic approximation of olivine single crystal accounts for 79.3 per cent of the norm of the tensor with isotropic moduli equal to $K = 109.8$ GPa and $G = 63.7$ GPa. The remaining anisotropic part represents 20.7 per cent of the norm of the tensor. The different elastic symmetry parts of the tensor are presented as percentages of the norm of the elastic tensor in the histogram of Fig. 1 using the following convention:

$$100 \text{ per cent} = N^{-2}(\mathbf{X})\left[N^2(\mathbf{X}_{\mathrm{tric}}) + N^2(\mathbf{X}_{\mathrm{mon}}) + N^2(\mathbf{X}_{\mathrm{ort}}) + N^2(\mathbf{X}_{\mathrm{tet}}) + N^2(\mathbf{X}_{\mathrm{hex}}) + N^2(\mathbf{X}_{\mathrm{iso}})\right]. \tag{4.1}$$

Anisotropic parts of the tensors are mainly hexagonal and orthorhombic. Most of the anisotropy is hexagonal (15.2 per cent), while the remaining 5.5 per cent is tetragonal and orthorhombic (first column of Fig. 1).

4.1.2 Enstatite

Enstatite is less anisotropic (9.2 per cent) than olivine as the isotropic part accounts for 90.8 per cent of the norm of the elastic tensor (moduli are $K = 108.3$ GPa and $G = 76.4$ GPa). Anisotropy is distributed between the hexagonal part (4.3 per cent) and the tetragonal/orthorhombic part (4.9 per cent). Addition of enstatite to the olivine decreases the total anisotropy as well as the orthorhombic part.

$$C_{IJ} = \begin{pmatrix} 225 & 54 & 72 & 0 & 0 & 0 \\ 54 & 214 & 53 & 0 & 0 & 0 \\ 72 & 53 & 178 & 0 & 0 & 0 \\ 0 & 0 & 0 & 78 & 0 & 0 \\ 0 & 0 & 0 & 0 & 82 & 0 \\ 0 & 0 & 0 & 0 & 0 & 76 \end{pmatrix} = \begin{pmatrix} 55 & 0 & 95 & 0 & 0 & 0 \\ 0 & -55 & -95 & 0 & 0 & 0 \\ 95 & -95 & 0 & 0 & 0 & 0 \\ 0 & 0 & 0 & -2 & 0 & 0 \\ 0 & 0 & 0 & 0 & 2 & 0 \\ 0 & 0 & 0 & 0 & 0 & 0 \end{pmatrix}_{\mathrm{O}}$$

$$+ \begin{pmatrix} 3.4 & -3.4 & 0 & 0 & 0 & 0 \\ -3.4 & 3.4 & 0 & 0 & 0 & 0 \\ 0 & 0 & 0 & 0 & 0 & 0 \\ 0 & 0 & 0 & 0 & 0 & 0 \\ 0 & 0 & 0 & 0 & 0 & 0 \\ 0 & 0 & 0 & 0 & 0 & -3.4 \end{pmatrix}_{\mathrm{T}} + \begin{pmatrix} 5.9 & 1.7 & 5.1 & 0 & 0 & 0 \\ 0 & 5.9 & 5.1 & 0 & 0 & 0 \\ 5.1 & 5.1 & -32.2 & 0 & 0 & 0 \\ 0 & 0 & 0 & 3.6 & 0 & 0 \\ 0 & 0 & 0 & 0 & 3.6 & 0 \\ 0 & 0 & 0 & 0 & 0 & 3.0 \end{pmatrix}_{\mathrm{H}} + \begin{pmatrix} 210.2 & 57.4 & 57.4 & 0 & 0 & 0 \\ 57.4 & 210.2 & 57.4 & 0 & 0 & 0 \\ 57.4 & 57.4 & 210.2 & 0 & 0 & 0 \\ 0 & 0 & 0 & 76.4 & 0 & 0 \\ 0 & 0 & 0 & 0 & 76.4 & 0 \\ 0 & 0 & 0 & 0 & 0 & 76.4 \end{pmatrix}_{\mathrm{I}}.$$

4.2 Depth variation of elastic symmetry in the upper mantle

Because elastic moduli of olivine and orthopyroxene depend on pressure and temperature, seismic anisotropy is expected to vary as a function of depth. To measure this effect, we have taken elastic moduli and their derivatives from Estey & Douglas (1986), assuming an aggregate of 70 per cent olivine $Fo_{93}Fa_7$ and 30 per cent orthopyroxene $En_{80}Fs_{20}$ (with the [010] axis parallel to the olivine [100] axis and the [100] axis parallel to the olivine [001] axis). The oceanic geotherm used is from Stacey (1977) and pressure and density profiles come from the

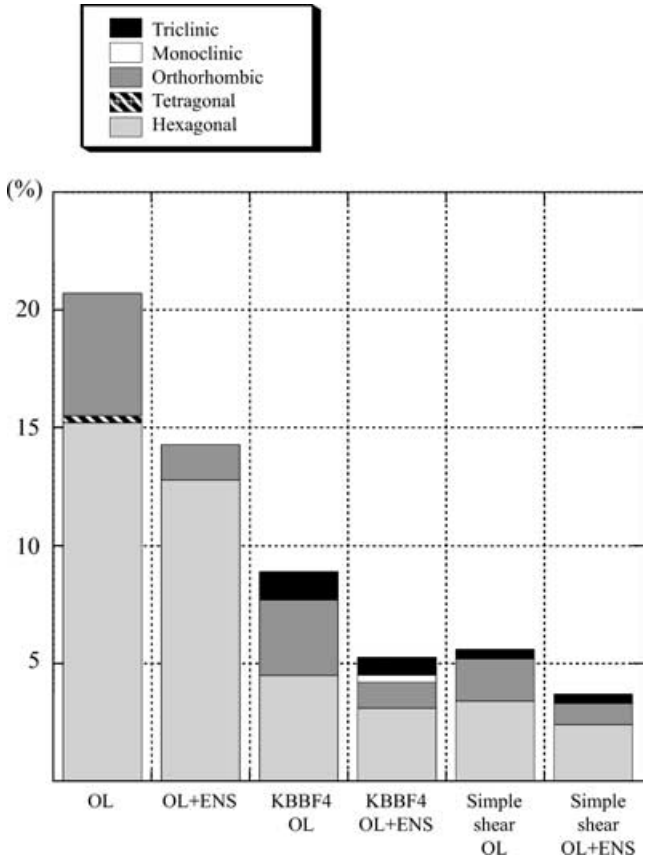

Figure 1. Decomposition of the elastic tensor, expressed in percentage of the total norm. OL denotes olivine single crystal (Section 4.1.1), OL + ENS represents 70 per cent OL and 30 per cent enstatite (Sections 4.1.1 and 4.1.2) with the enstatite [010]-axis parallel to the olivine [100]-axis and the enstatite [100]-axis parallel to the olivine [001]-axis. KBBF4 OL corresponds to olivine samples fabrics and KBBF4 OL + ENS to olivine and enstatite samples fabrics (Section 4.3). Simple shear case is a numerical deformation for finite strain $\varepsilon = 100$ per cent (Section 4.3).

Table 3. Symmetry decomposition as a function of depth in the upper mantle. Anisotropy (Anis.) and the hexagonal part (Hex.) decrease with depth while orthorhombic part (Orth.) is almost constant.

Depth (km)	K (GPa)	G (GPa)	Anis.	Orth.	Hex.
60	113	68	17.8	5.9	11.9
115	121	69	17.3	6.0	11.2
185	134	72	16.2	6.2	9.9
220	140	73	15.7	6.2	9.3
265	149	75	15.2	6.3	8.7
310	158	78	14.7	6.4	8.0
355	167	80	14.2	6.5	7.4
400	176	82	13.8	6.5	6.9

Preliminary Reference Earth Model (Dziewonski & Anderson 1981). Triclinic, monoclinic and tetragonal parts are negligible (less than 0.5 per cent). The orthorhombic part contributes to the same percentage of the tensor through the entire depth of the upper mantle (Table 3). The hexagonal part and the total anisotropy decrease with depth as isotropic moduli increase. The orthorhombic part becomes predominant when depth increases.

4.3 Symmetry of natural xenolith samples

We consider the olivine and orthopyroxene orientations based upon the microscopic analysis of the peridotite sample KBBF4 (Boullier & Nicolas 1975; Mainprice & Silver 1993). This garnet lherzolite has been collected in the South African Kaapvaal region at Bulfontein (Kimberly) and has a modal composition of 68 per cent olivine, 27 per cent enstatite, 2.4 per cent garnet and 2 per cent clinopyroxene. This kimberlite nodule was formed at a pressure of 3.5 GPa, a temperature of 900 °C at 120 km depth approximately 120–80 Ma (Mainprice & Silver 1993). This sample experienced first a large-strain ductile deformation followed by annealing in the upper mantle prior to a rapid eruption. Measurements of the orientation of 95 olivine crystals and 56 enstatite crystals have been performed.

The distribution of the orientations of olivine and enstatite results in the amplitude of anisotropy being lower than of single crystals. The ratio between the orthorhombic and the hexagonal part is slightly increased (fourth column of Fig. 1) and a triclinic part occurs.

4.4 Anisotropy of numerically deformed olivine aggregate

4.4.1 Symmetry

Kaminski & Ribe (2001) have developed a model for the evolution of LPO in olivine aggregates that deform by both intracrystalline slip (plastic deformation) and dynamic recrystallization. In this model, dynamic recrystallization implies that grains with a large density of dislocations lower their bulk strain energy by nucleating strain-free subgrains at a rate proportional to a dimensionless parameter λ^*. Grains with high energy are then invaded by grains with low energy by grain-boundary migration at a rate proportional to a dimensionless grain-boundary mobility M^*. Values of these two parameters are constrained to $\lambda^* > 3$ and $M^* = 125 \pm 75$ in Kaminski & Ribe (2001) by comparison with the LPO produced in laboratory experiments. The best-fitting values are $\lambda^* = 5$ for nucleation and $M^* = 50$ for mobility. The aggregate is constituted by 15^3 grains (70 per cent olivine and 30 per cent enstatite). Three active slip systems (010)[100], (001)[100] and (010)[001] with a non-newtonian rheology exponent 3.5 are considered for the plastic deformation of olivine at high temperature. Critical shear stresses that are adimensionalized to the weakest slip system are $\tau_1 = 1$, $\tau_2 = 2$ and $\tau_3 = 3$ (Kaminski & Ribe 2001). Enstatite has only one slip system. Voigt average elastic tensors of the aggregates for simple shear deformation and uniaxial compression are analysed.

Simple shear deformation of $\varepsilon = 100$ per cent decreases the norm of the anisotropic part of the tensor (5.6 per cent) present in an olivine single crystal while preserving the relative magnitudes of the different symmetry parts (fifth column of Fig. 1). A slight monoclinic/triclinic component is also present as the result of the statistical distribution of orientations of olivine crystals within the aggregate.

4.4.2 Deformation and anisotropy

Figs 2 and 3 show the evolution of the symmetry composition of numerically deformed olivine aggregates versus finite strain $\varepsilon = 2\dot{\varepsilon}t$ for a simple shear deformation. Introducing the long axis a and the short axis c of the finite strain ellipsoid, we get $\ln(a/c) = \varepsilon$ for a simple shear deformation and $\ln(a/c) = \varepsilon/2$ for an uniaxial compression (Ribe & Yu 1991). In simple shear deformation (Fig. 2), the dominant parts are hexagonal and orthorhombic. In uniaxial compression (Fig. 3), the anisotropic part is dominated by the hexagonal part. However, while the [100]-axis is the symmetry axis for the hexagonal part of the olivine crystal, the symmetry axis becomes the [010]-axis when olivine aggregates are deformed by uniaxial compression.

These curves allow a comparison between synthetic and natural olivine aggregate fabrics. Anisotropy of the KBBF4 sample is 8.4 per cent with a predominant orthorhombic part (Fig. 1), which could correspond to a 150 per cent simple shear deformation (Fig. 2). Bystricky *et al.* (2000) have calculated from laboratory experiments a *P*-wave anisotropy of respectively 3.1 and 14.9 per cent for a 50 and 500 per cent simple shear deformation. Our results fall within this range.

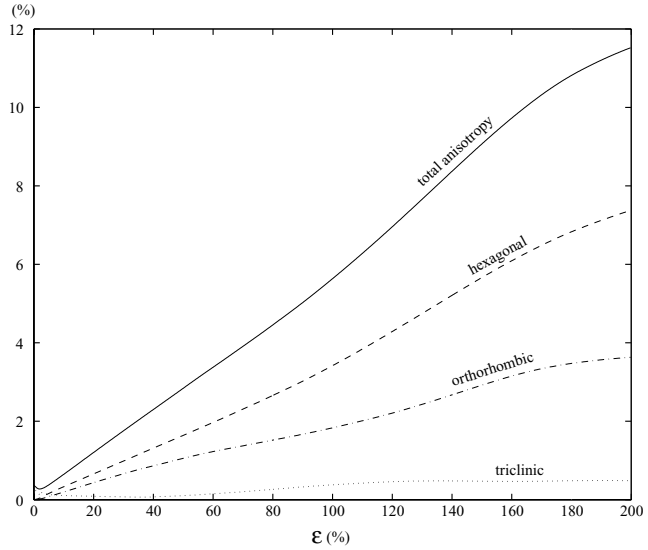

Figure 2. Evolution of the same decomposition as in Fig. 1 for simple shear deformation with finite strain ε. Monoclinic and tetragonal parts are negligible (less than 0.1 per cent). Anisotropy is the result of hexagonal and orthorhombic parts.

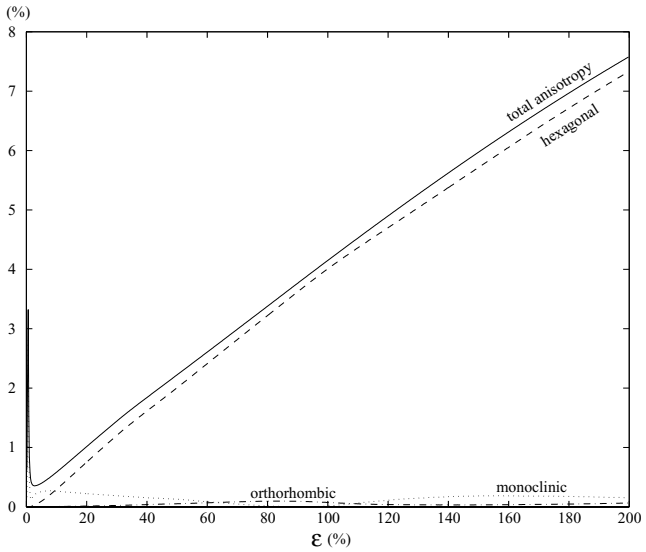

Figure 3. Same as Fig. 2 but for an uniaxial compression (triclinic and tetragonal parts are less than 0.1 per cent) in which anisotropy is almost equal to the hexagonal part. In the early stage of deformation, a monoclinic peak appears as the [100] and [001] axes rotate into the plane perpendicular to the compression axis without any specific symmetry. Then their orientations in this plane become isotropic and the hexagonal symmetry develops.

4.5 Hexagonal approximation

The symmetry decomposition method allows one to find the optimum equivalent hexagonal medium. The bias introduced by assuming hexagonal symmetry is investigated in this section.

Fig. 4 shows the influence of the simple shear finite strain and of the aggregate composition on the SWS induced by the hexagonal part (propagation perpendicular to the hexagonal axis). SWS shows a linear dependence with finite strain up to 150 per cent deformation, beyond which saturation occurs at a level of 1.7 s compatible with SWS observations. The presence of enstatite globally decreases splitting.

Fig. 5 inspects the bias introduced by assuming hexagonal symmetry for a 100 per cent simple shear deformation. Assuming a horizontal hexagonal axis, SWS effects for a vertical propagation of 100 km are shown for a rotation of the tensor around this horizontal direction. Considering solely the hexagonal part yields a constant SWS. Taking into account the orthorhombic part gives variations of the same order of magnitude as the ones obtained by taking the enstatite into account. Splitting variation resulting from the rotation of the orthorhombic tensor around the fastest axis has an amplitude of 0.3 s. Introducing enstatite in the aggregates decreases the splitting to 0.4 s and smooths splitting variations resulting from orthorhombicity to an amplitude of 0.2 s. Each of these two effects therefore represents less than half of typical delay times measured by studying *SKS* splitting.

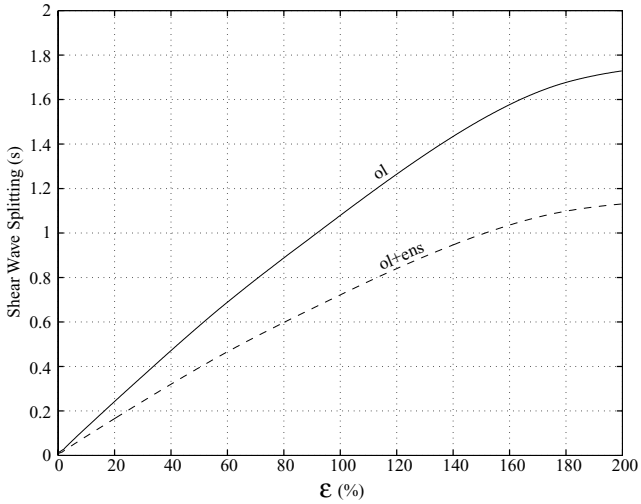

Figure 4. Evolution of SWS as a result of the hexagonal part of the tensor with finite strain ε. Waves propagate vertically across a 100-km-thick layer with a horizontal hexagonal axis. Deformation is simple shear and the two cases are for olivine elastic tensor (ol) and for 70 per cent olivine and 30 per cent enstatite (ol + ens). Elastic coefficients and densities come from Anderson & Isaak (1995) for olivine and Bass (1995) for enstatite.

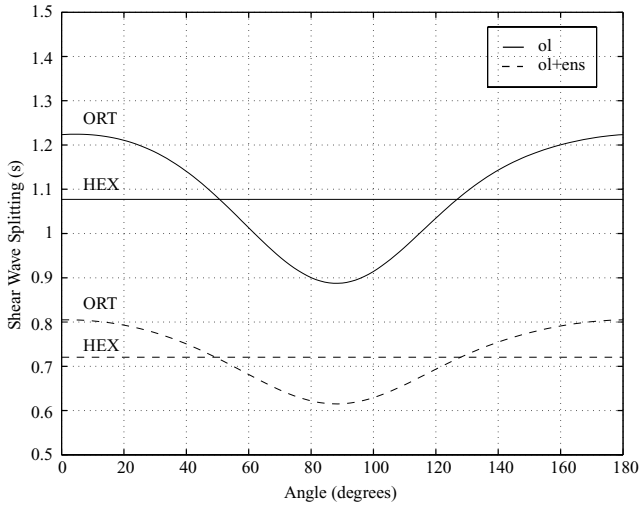

Figure 5. Influence of the orthorhombic component on SWS using elastic tensors ol and ol + ens (same composition as the last two columns of Fig. 1) for a simple shear deformation $\varepsilon = 100$ per cent. The configuration is the same as in Fig. 4. HEX denotes the hexagonal part while ORT is the hexagonal plus the orthorhombic part. The angle is the rotation angle of the tensors around the horizontal fast axis direction.

5 CONCLUSION

Vectorial description of elastic tensors is convenient for their decomposition and approximation into the different elastic symmetry classes. For approximating the elastic tensor, we propose a simple and direct projection method that leaves the isotropic component unaffected. Provided the elastic tensor is close to orthorhombic, our analysis of symmetry composition of an elastic tensor yields proper symmetry approximations of elastic media. Typical mantle aggregates sampled at the surface are mainly hexagonal and orthorhombic with a total anisotropy around 5 per cent. The relation between SWS and intensity of deformation allows a calibration of the deformation experienced by natural samples at least for simple shear and uniaxial compression.

ACKNOWLEDGMENTS

We would like to thank Neil Ribe and Edouard Kaminski for their critical reading of the first version of the manuscript and their suggestions that greatly helped to improve it. We also thank Véronique Farra and Albert Tarantola for discussions about the way to represent an elastic tensor. This research was supported by an INSU grant 'Intérieur de la Terre'.

REFERENCES

Anderson, D.L., 1989. *Theory of the Earth,* Blackwell Scientific Publications, Boston, MA.

Anderson, O.L. & Isaak, D.G., 1995. Elastic Constants of Mantle Minerals at High Temperature, in, *Mineral Physics and Crystallography, A Handbook of Physical Constants,* ed. Ahrens, T.J., AGU, Washington, DC.

Arts, R.J., 1993. A study of general anisotropic elasticity in rocks by wave propagation—Theoretical and experimental aspects -, *PhD thesis,* University Pierre & Marie Curie, Paris.

Arts, R.J., Helbig, K. & Rasolofosaon, P.N.J., 1991. General Anisotropic Elastic Tensor in Rocks: Approximation, Invariants and Particular Directions, *61st Annual International Meeting, Society of Exploration Geophysicists, Expanded Abstracts,* ST2.4, pp. 1534–1537, SEG, Tulsa.

Backus, G.E., 1970. A geometrical picture of anisotropic elastic tensors, *Reviews of Geophysics and Space Physics,* **8,** 633–671.

Bass, J.D., 1995. Elasticity of Minerals, Glasses, and Melts, in, *Mineral Physics and Crystallography, A Handbook of Physical Constants,* ed. Ahrens, T.J., AGU, Washington, DC.

Bennett, H.F., 1972. A Simple Seismic Model for Determining Principal Anisotropic Direction, *J. geophys. Res.,* **77,** 3078–3080.

Blackman, D.K. & Kendall, J.M., 2002. Seismic Anisotropy of the Upper Mantle: 2. Predictions for Current Plate Boundary Flow Models, *Geochem. Geophys. Geosyst.,* **3**(9), 8602, 101029/2001GC000247.

Blackman, D.K., Wenk, H.R. & Kendall, J.M., 2002. Seismic Anisotropy of the Upper Mantle, 1, Factors That Affect Mineral Texture and Effective Elastic Properties, *Geochem. Geophys. Geosyst.,* **3**(9)**,** 8601, 101029/2001GC000248.

Boullier, A.M. & Nicolas, A., 1975. Classification of textures and fabrics of peridotite xenoliths from South African kimberlites, *Phys. Chem. Earth,* **9,** 467–475.

Bystricky, M., Kunze, K., Burlini, L. & Burg, J.-P., 2000. High shear strain of olivine aggregates: rheological and seismic consequences, *Science,* **290,** 1564–1567.

Cowin, S.C. & Mehrabadi, M.M., 1987. On the identification of material symmetry for anisotropic elastic materials, *Quaterly J. Mechanics and Applied Mathematics,* **40,** 451–476.

Dziewonski, A.M. & Anderson, D.L., 1981. Preliminary Reference Earth Model, *Phys. Earth planet. Int.,* **25,** 297–356.

Estey, L.H. & Douglas, B.J., 1986. Upper Mantle Anisotropy: A Preliminary Model, *J. geophys. Res.,* **91**(B11), 11 393–11 406.

Favier, N. & Chevrot, S., 2003. Sensitivity kernels for shear-wave splitting in transverse isotropic media, *Geophys. J. Int.,* **153,** 213–228.

Fedorov, F.I., 1968. *Theory of Elastic Waves in Crystals,* Plenum Press, New York.

Helbig, K., 1994. *Foundations of Anisotropy for Exploration Seismics,* Handbook of Geophysical Exploration, Vol. 22, Pergamon, London.

Helbig, K., 1995. Representation and Approximation of elastic tensor, *6th International Workshop on Seismic Anisotropy (Trondheim, 1994), Expanded Abstracts,* P1-1, pp. 37–75.

Kaminski, E. & Ribe, N.M., 2001. A kinematic model for recrystallization and texture development in olivine polycrystals, *Earth planet. Sci. Lett.,* **189,** 253–267.

Kaminski, E. & Ribe, N.M., 2002. Time scales for the evolution of seismic anisotropy in mantle flow, *G-cubed,* **3,** 10.1029/2001GC000222 and, *Geochem. Geophys. Geosyst.,* **3**(8), 1051, 101029/2001GC000222.

Kelvin, Lord (William Thomson), 1856. Elements of a mathematical theory of elasticity, Part I, On stresses and strains, *Phil. Trans. R. Soc.,* **166,** 481–498.

Mainprice, D. & Silver, P.G., 1993. Interpretation of SKS-waves using samples from the subcontinental lithosphere, *Phys. Earth planet. Int.,* **78,** 257–280.

Montagner, J.P. & Nataf, H.C., 1986. On the inversion for the azimuthal anisotropy of surfaces waves, *J. geophys. Res.,* **91,** 511–520.

Montagner, J.P. & Nataf, H.C., 1988. Vectorial tomography I: Theory, *Geophys. J. R. astr. Soc.,* **94,** 295–307.

Montagner, J.P. & Tanimoto, T., 1991. Global upper mantle tomography of seismic velocities and anisotropies, *J. geophys. Res.,* **96,** 20 337–20 351.

Nicolas, A. & Christensen, N.I., 1987. Formation of anisotropy in upper mantle peridotites: a review, in, *Composition, Structure and Dynamics of the Lithosphere-Asthenosphere System, Geodyn. Monogr. Ser.,* 16, pp. 111–123, eds Fuchs, K. & Froidevaux, C., AGU, Washington, DC.

Ribe, N.M., 1992. On the relation between seismic anisotropy and finite strain, *J. geophys. Res.,* **97**(B6), 8737–8747.

Ribe, N.M. & Yu, Y., 1991. A theory for plastic deformation and textural evolution of olivine polycrystals, *J. geophys. Res.,* **96**(B5), 8325–8335.

Silver, P.G. & Chan, W.W., 1991. Shear wave splitting and subcontinental mantle deformation, *J. geophys. Res.,* **96,** 16 429–16 454.

Smith, M.L. & Dahlen, F.A., 1973. The azimuthal dependence of Love and Rayleigh wave propagation in a slightly anisotropic medium, *J. geophys. Res.,* **78,** 3321–3333.

Stacey, F.D., 1977. A Thermal Model of the Earth, *Phys. Earth planet. Int.,* **15,** 341–348.

Trampert, J. & Woodhouse, J.H., 1995. Global phase velocity maps of Love and Rayleigh waves between 40 and 150 seconds, *Geophys. J. Int.,* **122,** 675–690.

Wenk, H.R. & Tomé, C.N., 1999. Modeling dynamic recrystallization of olivine aggregates deformed in simple shear, *J. geophys. Res.,* **104,** 25 513–25 527.

Zhang, S. & Karato, S., 1995. Lattice preffered orientation of olivine aggregates in simple shear, *Nature,* **375,** 774–777.

APPENDIX A: ORTHOGONAL PROJECTORS

Each general projector p is represented by a matrix $\mathbf{M}$ in the 21-D vectorial space described by the orthonormal basis given in Table 1. The projection of any vector $\mathbf{X}$ on a higher symmetry subspace of dimension N_H is given by $\mathbf{X}_H = \mathbf{M}.\mathbf{X}$. Projectors are found according to the relation (3.3) and using the properties that an orthogonal projector p is such that $p^2 = p$ and that its matrix representation on an orthonormal basis is symmetric. Necessary conditions for a vector $\mathbf{X}$ to belong to a subspace H are also given below. These conditions are cumulative with increasing symmetry order.

A1 Projection p_1 onto monoclinic symmetry ($N_H = 13$)

For monoclinic symmetry:

$$X_{10} = X_{11} = X_{13} = X_{14} = X_{16} = X_{17} = X_{19} = X_{20} = 0. \tag{A1}$$

$\mathbf{M^{(1)}}$ is the unit 21×21 square matrix but with diagonal coefficients $M^{(1)}_{i,i}$, with $i = 10, 11, 13, 14, 16, 17, 19, 20$ equal to zero.

A2 Projection p_2 onto orthorhombic symmetry ($N_H = 9$)

For orthorhombic symmetry:

$$X_{12} = X_{15} = X_{18} = X_{21} = 0. \tag{A2}$$

$\mathbf{M^{(2)}}$ is the unit 21×21 square matrix with diagonal coefficients $M^{(2)}_{i,i}$ with $i = 10, \ldots, 21$ equal to zero. In the following, projectors on symmetry classes higher than orthorhombic will be presented by only their upper left 9×9 square matrix because the remaining part only contains zeros.

A3 Projection p_3 onto tetragonal symmetry ($N_H = 6$)

For tetragonal symmetry:

$$X_1 = X_2, \quad X_4 = X_5, \quad X_7 = X_8 \tag{A3}$$

and the projection matrix is given by

$$\mathbf{M^{(3)}} = \begin{bmatrix} 1/2 & 1/2 & 0 & 0 & 0 & 0 & 0 & 0 & 0 \\ 1/2 & 1/2 & 0 & 0 & 0 & 0 & 0 & 0 & 0 \\ 0 & 0 & 1 & 0 & 0 & 0 & 0 & 0 & 0 \\ 0 & 0 & 0 & 1/2 & 1/2 & 0 & 0 & 0 & 0 \\ 0 & 0 & 0 & 1/2 & 1/2 & 0 & 0 & 0 & 0 \\ 0 & 0 & 0 & 0 & 0 & 1 & 0 & 0 & 0 \\ 0 & 0 & 0 & 0 & 0 & 0 & 1/2 & 1/2 & 0 \\ 0 & 0 & 0 & 0 & 0 & 0 & 1/2 & 1/2 & 0 \\ 0 & 0 & 0 & 0 & 0 & 0 & 0 & 0 & 1 \end{bmatrix}.$$

A4 Projection p_4 onto hexagonal symmetry ($N_H = 5$)

For hexagonal symmetry:

$$X_1 - X_6/\sqrt{2} = X_9. \tag{A4}$$

A vector $\mathbf{X}$ in the tetragonal symmetry class has the form

$$\mathbf{X} = (X_1, X_1, X_3, X_4, X_4, X_6, X_7, X_7, X_9). \tag{A5}$$

A tetragonal vector perpendicular to the hexagonal subspace must have a scalar product with $\mathbf{X}$ equal to a multiple of $X_1 - X_6/\sqrt{2} - X_9$. Therefore, the normalized vector

$$\mathbf{X}_N = \frac{1}{\sqrt{2}}\left(1/2, 1/2, 0, 0, 0, -1/\sqrt{2}, 0, 0, -1\right) \tag{A6}$$

can be used to define the projector from the tetragonal space onto the hexagonal subspace according to the relation (3.3):

$$p(\mathbf{X}) = I(X) - (\mathbf{X}\cdot\mathbf{X}_N)\mathbf{X}_N, \tag{A7}$$

where I is the identity operator. The unique general projector p_4 on the hexagonal space is given by $p \circ p_3$, where $\circ$ denotes the composition. The projection matrix is then

$$\mathbf{M}^{(4)} = \begin{bmatrix} 3/8 & 3/8 & 0 & 0 & 0 & 1/4\sqrt{2} & 0 & 0 & 1/4 \\ 3/8 & 3/8 & 0 & 0 & 0 & 1/4\sqrt{2} & 0 & 0 & 1/4 \\ 0 & 0 & 1 & 0 & 0 & 0 & 0 & 0 & 0 \\ 0 & 0 & 0 & 1/2 & 1/2 & 0 & 0 & 0 & 0 \\ 0 & 0 & 0 & 1/2 & 1/2 & 0 & 0 & 0 & 0 \\ 1/4\sqrt{2} & 1/4\sqrt{2} & 0 & 0 & 0 & 3/4 & 0 & 0 & -1/2\sqrt{2} \\ 0 & 0 & 0 & 0 & 0 & 0 & 1/2 & 1/2 & 0 \\ 0 & 0 & 0 & 0 & 0 & 0 & 1/2 & 1/2 & 0 \\ 1/4 & 1/4 & 0 & 0 & 0 & -1/2\sqrt{2} & 0 & 0 & 1/2 \end{bmatrix}.$$

Applying projector p_4 to a 21-D vector $\mathbf{X}$ will produce the same hexagonal approximation as the one given by Arts (1993):

$$C_{11}^{\text{hex}} = C_{22}^{\text{hex}} = \frac{3}{8}(C_{11} + C_{22}) + \frac{1}{4}C_{12} + \frac{1}{2}C_{66}, \tag{A8}$$

$$C_{33}^{\text{hex}} = C_{33}, \tag{A9}$$

$$C_{23}^{\text{hex}} = C_{13}^{\text{hex}} = \frac{1}{2}(C_{13} + C_{23}), \tag{A10}$$

$$C_{12}^{\text{hex}} = \frac{1}{8}(C_{11} + C_{22}) + \frac{3}{4}C_{12} - \frac{1}{2}C_{66}, \tag{A11}$$

$$C_{44}^{\text{hex}} = \frac{1}{2}(C_{44} + C_{55}), \tag{A12}$$

$$C_{66}^{\text{hex}} = \frac{1}{2}\left(C_{11}^{\text{hex}} - C_{12}^{\text{hex}}\right) = \frac{1}{8}(C_{11} + C_{22}) - \frac{1}{4}C_{12} + \frac{1}{2}C_{66}. \tag{A13}$$

A5 Projection p_5 onto the isotropic space ($N_H = 2$)

For an isotropic material:

$$X_1 - X_3 = 0, \tag{A14}$$

$$X_4 - \sqrt{2}(X_1 - X_9) = 0, \tag{A15}$$

$$X_7 - X_9 = 0. \tag{A16}$$

A vector in the hexagonal symmetry class has the form

$$\mathbf{X} = \left(X_1, X_1, X_3, X_4, X_4, \sqrt{2}(X_1 - X_9), X_7, X_7, X_9\right). \tag{A17}$$

Any hexagonal vector $(a, a, b, 0, 0, \sqrt{2}(a-c), 0, 0, c)$ that is perpendicular to the subspace $X_1 - X_3 = 0$ must have a scalar product with $\mathbf{X}$ equal to $X_1 - X_3$ equal to a multiple of $X_1 - X_3$. This condition gives $a = 3/8$, $b = -1$ and $c = 1/4$. Therefore, the normalized vector

$$\mathbf{X}_N = \sqrt{\frac{8}{11}}\left(3/8, 3/8, -1, 0, 0, \sqrt{2}/8, 0, 0, 1/4\right) \tag{A18}$$

can be used to determine the projector on the subspace defined by $X_1 - X_3 = 0$:

$$p(\mathbf{X}) = I(\mathbf{X}) - (\mathbf{X}\cdot\mathbf{X}_N)\mathbf{X}_N, \tag{A19}$$

where I is the identity operator. The unique general projector on the subspace $X_1 - X_3 = 0$ is given by $p \circ p_4$. Taking a similar approach for the relations (A15) and (A16), we get the general projector onto isotropic symmetry:

$$\mathbf{M}^{(5)} = \begin{bmatrix} 3/15 & 3/15 & 3/15 & \sqrt{2}/15 & \sqrt{2}/15 & \sqrt{2}/15 & 2/15 & 2/15 & 2/15 \\ 3/15 & 3/15 & 3/15 & \sqrt{2}/15 & \sqrt{2}/15 & \sqrt{2}/15 & 2/15 & 2/15 & 2/15 \\ 3/15 & 3/15 & 3/15 & \sqrt{2}/15 & \sqrt{2}/15 & \sqrt{2}/15 & 2/15 & 2/15 & 2/15 \\ \sqrt{2}/15 & \sqrt{2}/15 & \sqrt{2}/15 & 4/15 & 4/15 & 4/15 & -\sqrt{2}/15 & -\sqrt{2}/15 & -\sqrt{2}/15 \\ \sqrt{2}/15 & \sqrt{2}/15 & \sqrt{2}/15 & 4/15 & 4/15 & 4/15 & -\sqrt{2}/15 & -\sqrt{2}/15 & -\sqrt{2}/15 \\ \sqrt{2}/15 & \sqrt{2}/15 & \sqrt{2}/15 & 4/15 & 4/15 & 4/15 & -\sqrt{2}/15 & -\sqrt{2}/15 & -\sqrt{2}/15 \\ 2/15 & 2/15 & 2/15 & -\sqrt{2}/15 & -\sqrt{2}/15 & -\sqrt{2}/15 & 1/5 & 1/5 & 1/5 \\ 2/15 & 2/15 & 2/15 & -\sqrt{2}/15 & -\sqrt{2}/15 & -\sqrt{2}/15 & 1/5 & 1/5 & 1/5 \\ 2/15 & 2/15 & 2/15 & -\sqrt{2}/15 & -\sqrt{2}/15 & -\sqrt{2}/15 & 1/5 & 1/5 & 1/5 \end{bmatrix}.$$

From the expression of $\mathbf{M}^{(5)}$, it can be seen that the incompressibility modulus K and the shear modulus G are combinations of the traces of the dilatational tensor $d_{ij} = c_{ijkk}$ and the Voigt tensor $v_{ik} = c_{ijkj}$, which are two scalar invariants of the fourth rank tensor c_{ijkl}:

$$K = d_{jj}/9, \tag{A20}$$

$$G = (3v_{kk} - d_{jj})/30. \tag{A21}$$

These analytical relations were already proposed by Fedorov (1968), Backus (1970) and Arts (1993). The resulting 21-D isotropic vector has only its first nine components that are non-zero:

$$X_1 = K + 4G/3, \tag{A22}$$

$$X_2 = K + 4G/3, \tag{A23}$$

$$X_3 = K + 4G/3, \tag{A24}$$

$$X_4 = \sqrt{2}(K - 2G/3), \tag{A25}$$

$$X_5 = \sqrt{2}(K - 2G/3), \tag{A26}$$

$$X_6 = \sqrt{2}(K - 2G/3), \tag{A27}$$

$$X_7 = 2G, \tag{A28}$$

$$X_8 = 2G, \tag{A29}$$

$$X_9 = 2G. \tag{A30}$$

For any projection, isotropic parameters K and G are not affected by the removal of the lower symmetry parts.